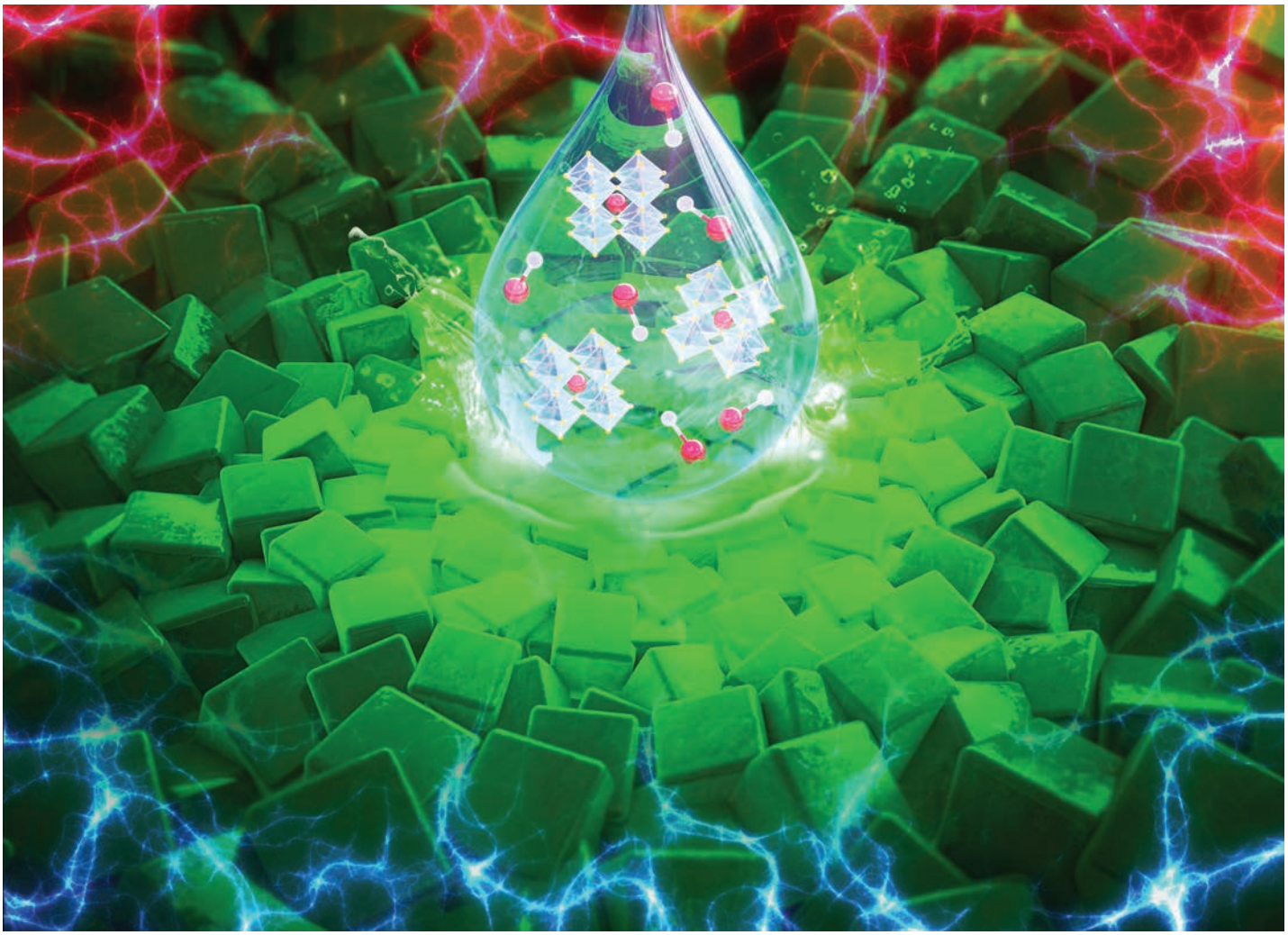

Showcasing research from the School of Materials Science Engineering/KIST-UNIST Ulsan Center for Convergent Materials, Ulsan National Institute of Science and Technology (UNIST), Ulsan, Korea.

Title: High-performance perovskite light-emitting diodes *via* morphological control of perovskite films

This study suggests a simple method for the morphology control of perovskite films. The deposition of a dense and uniform perovskite layer with full surface coverage was achieved by adding a small amount of HBr to the perovskite precursor, which facilitated full coverage electroluminescence of the fabricated perovskite light-emitting diode (PeLED), resulting in a highly efficient PeLED.

As featured in:

See Myoung Hoon Song *et al.* *Nanoscale*, 2016, **8**, 7036.

ROYAL SOCIETY OF CHEMISTRY

www.rsc.org/nanoscale

Registered charity number: 207890

Nanoscale

PAPER

View Article Online
View Journal | View Issue

Cite this: *Nanoscale*, 2016, **8**, 7036

High-performance perovskite light-emitting diodes *via* morphological control of perovskite films†

Jae Choul Yu,‡ Da Bin Kim,‡ Eui Dae Jung, Bo Ram Lee and Myoung Hoon Song*

Received 18th August 2015,
Accepted 10th November 2015

DOI: 10.1039/c5nr05604g

www.rsc.org/nanoscale

Solution-processable perovskite materials have garnered tremendous attention because of their excellent charge carrier mobility, possibility of a tunable optical bandgap, and high photoluminescence quantum efficiency (PLQE). In particular, the uniform morphology of a perovskite film is the most important factor in realizing perovskite light-emitting diodes (PeLEDs) with high efficiency and full-coverage electroluminescence (EL). In this study, we demonstrate highly efficient PeLEDs that contain a perovskite film with a uniform morphology by introducing HBr into the perovskite precursor. The introduction of HBr into the perovskite precursor results in a perovskite film with a uniform, continuous morphology because the HBr increases the solubility of the inorganic component in the perovskite precursor and reduces the crystallization rate of the perovskite film upon spin-coating. Moreover, PeLEDs fabricated using perovskite films with a uniform, continuous morphology, which were deposited using 6 vol% HBr in a dimethylformamide (DMF)/hydrobromic acid (HBr) cosolvent, exhibited full coverage of the green EL emission. Finally, the optimized PeLEDs fabricated with perovskite films deposited using the DMF/HBr cosolvent exhibited a maximum luminance of 3490 cd m^{-2} (at 4.3 V) and a luminous efficiency of 0.43 cd A^{-1} (at 4.3 V).

1. Introduction

Organic–inorganic hybrid semiconductors such as quantum dots and perovskite materials[1–3] have attracted interest because of their excellent properties; these properties include superior charge carrier mobility compared to that of organic materials, a tunable optical bandgap, and easy solution processing, which raises the possibility of large-area displays and flexible device applications.[4,5] Recently, solution-processable perovskite films with a photoluminescence quantum efficiency (PLQE) as high as 70% have been reported; the high PLQE of these films makes them promising semiconductor candidates for LED applications.[6] Moreover, the perovskite materials used in solar cells have also demonstrated excellent photovoltaic (PV) performance, with efficiencies ranging from 4 to 19.3%.[7,8]

The Cambridge group first reported green and infrared emissive perovskite light-emitting diodes (PeLEDs) whose bandgaps could be varied through changes in their chemical composition. These PeLEDs achieved a luminescence of 364 cd m^{-2} and a radiance of 6.8 W sr^{-1} m^{-2}.[3] Moreover, Kim *et al.* demonstrated highly efficient PeLEDs with a luminescence of 417 cd m^{-2} by modifying the workfunction of PEDOT:PSS using a self-organized buffer hole–injection layer (Buf-HIL), which reduced the hole–injection barrier between the PEDOT:PSS and the perovskite emissive layer.[9] Recently, the Cambridge group also demonstrated a conventional structured PeLED fabricated using spatial atmospheric atomic layer-deposited (SAALD) $Zn_{1-x}Mg_xO$ as an electron transport layer (ETL).[10] Their PeLED with an F8 layer exhibited a maximum luminescence efficiency of 364 cd m^{-2}, whereas their PeLED with an SAALD layer exhibited a significantly improved maximum luminescence of 550 cd m^{-2} and enhanced air stability. One of the most important criteria for highly efficient perovskite optoelectronic devices is the uniform morphology of the perovskite crystal.[11–14] However, previous papers regarding PeLEDs have not demonstrated a correlation between the perovskite morphology and the electroluminescence (EL) image in PeLEDs.

Here, we report the fabrication of a highly efficient perovskite-based green LED *via* the morphological control of methylammonium lead tribromide ($CH_3NH_3PbBr_3$, $MAPbBr_3$) films using a dimethylformamide (DMF)/hydrobromic acid

School of Materials Science Engineering/KIST-UNIST Ulsan Center for Convergent Materials, Ulsan National Institute of Science and Technology (UNIST), UNIST-gil 50, Ulsan, 689-798, Republic of Korea. E-mail: mhsong@unist.ac.kr

†Electronic supplementary information (ESI) available: Viscosity, top view and cross-sectional SEM images of the $MAPbBr_3$ film, energy diagram and device characteristics of PeLEDs. See DOI: 10.1039/c5nr05604g

‡These authors contributed equally.

(HBr) cosolvent through a 1-step spin-coat method. The optimized $MAPbBr_3$-based PeLED fabricated using the DMF/HBr cosolvent method exhibited a maximum luminance of 3490 cd m^{-2} (at 4.3 V) and a maximum luminous efficiency of 0.43 cd A^{-1} (at 4.3 V). The high efficiency of the planar PeLED is due to both the uniform morphology of $MAPbBr_3$ with full surface coverage and the optimized thicknesses of the $MAPbBr_3$ and ETL polymer layers. The deposition of a uniform and dense $MAPbBr_3$ layer with full surface coverage was achieved by adding an optimum amount of HBr to the perovskite precursor, and the full coverage of the green EL due to the highly uniform morphology of the perovskite layer was confirmed by optical microscopy.

2. Experimental

2.1 Materials

SPB-02 T polymer (product number: A.80827.0001) was purchased from Merck Co. and was used without purification. The CH_3NH_3Br synthesis and the preparation of the $CH_3NH_3PbBr_3$ solution have been described elsewhere.[15]

2.2 Device fabrication

For the fabrication of PeLEDs (ITO/PEDOT:PSS/$MAPbBr_3$/SPB-02 T/LiF/Ag), PEDOT:PSS was spin-coated onto a cleaned ITO/glass substrate at 5000 rpm for 45 s and subsequently annealed at 140 °C for 10 min. The $MAPbBr_3$ precursor (37.8 wt% MABr and $PbBr_2$ 1 : 1 molar ratio in *N*,*N*-dimethylformamide) solution with an aqueous HBr (48 wt%) solution in a volume ratio from 0 to 10 vol% were spin-coated onto the PEDOT:PSS-coated ITO/glass substrates at 3000 rpm for 60 s and annealed at 100 °C for 5 min under inert conditions. The electron transport layer was fabricated by coating SPB-02 T (blue copolymer) solution dispersed in chlorobenzene (0.45–0.72 wt%). Finally, LiF (1 nm) and silver (80 nm) were deposited by the vacuum thermal evaporation method using a 5-pixel mask. The active area of the device was 13.5 mm^2. The devices were encapsulated and legged before testing.

2.3 Characterization of $MAPbBr_3$ films and PeLEDs

The PeLED measurements were performed using a Keithley 2400 source measurement unit and a Konica Minolta spectroradiometer (CS-2000, Minolta Co.).[15] Scanning electron microscopy (Nanonova 230, FEI) was used to observe the morphology of the $MAPbBr_3$ films. XRD patterns were obtained from the samples of $MAPbBr_3$ with the HBr (0–10 vol%) cosolvent deposited onto the PEDOT:PSS substrate; the patterns were recorded using an X-ray diffractometer (D8 Advance, Bruker) equipped with a Cu-Kα radiation source (λ = 1.5405 Å). A step size of 0.01° was chosen with an acquisition time as high as 5 min deg^{-1}. EL microscopy images were obtained from the samples of PeLEDs using an optical microscope (IX81, Olympus).

3. Results and discussion

3.1 Device structure

Fig. 1(a) shows a schematic of the device structure (ITO/PEDOT:PSS/$MAPbBr_3$/SPB-02 T/LiF/Ag) used in the PeLED, and Fig. 1(b) shows a cross-sectional image of the complete PeLED, which is composed of indium tin oxide (ITO) as the anode, PEDOT:PSS as the transport layer (HTL), $MAPbBr_3$ with the DMF/HBr cosolvent as the perovskite emissive layer, SPB-02 T (blue copolymer, Merck Co.) as the ETL, and LiF/Al as the cathode. Fig. S1† shows the energy-level diagram of the fabricated PeLED. SPB-02 T is a commercial material, the material information including the structure and the energy level unfortunately is unknown. Thus, the energy level of SPB-02 T was inferred from that of the SPW-111 co-polymer (Merck Co.) with a similar structure.[16] The fabrication of the PeLEDs with the DMF/HBr cosolvent is described in detail in the Experimental section.

3.2 Viscosity measurement

Morphological control of perovskite films is important in improving device performance.[15] Thus, slow crystallization rates lead to the formation of a thinner perovskite film with full surface coverage because of the retarded nucleation time. The addition of an acid in the perovskite precursor solution is well known to slow the crystallization rate and improve the solubility of the solution through the enhanced solubility of the inorganic component.[17,18] Thus, HBr was added to the $MAPbBr_3$ precursor solution to obtain a $MAPbBr_3$ film with full surface coverage. In addition, the viscosity was measured to support the slow crystallization rate, which increased linearly with increasing HBr concentration, as shown in Fig. S2.† As a result, the crystallization rate of the perovskite film was

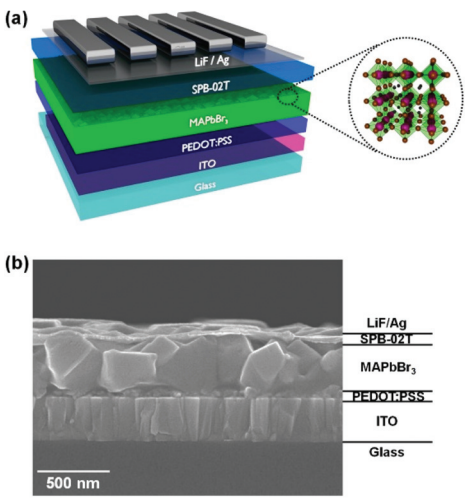

Fig. 1 (a) Schematic of the PeLED device with a fully coated perovskite layer. (b) Scanning electron micrograph cross-sectional image of the complete device with a perovskite layer prepared using 6 vol% of HBr in the DMF/HBr cosolvent.

reduced upon spin-coating; thus, a dense $MAPbBr_3$ film with greater surface coverage was fabricated on a PEDOT:PSS-coated ITO/glass substrate.

3.3 Scanning electron microscopy

To confirm the dense and full coverage of the $MAPbBr_3$ film, the morphology of the $MAPbBr_3$ films, which were deposited on PEDOT:PSS-coated ITO/glass substrates by spin-coating using different concentrations of HBr (0–10 vol%) in the DMF/HBr cosolvent, was observed using a scanning electron microscope (SEM); the resulting micrographs are shown in Fig. 2. The $MAPbBr_3$ films prepared using 0–4 vol% of HBr in the DMF/HBr cosolvent appeared to partially cover the substrate with islands and voids with submicron distances between them, as shown in Fig. 2(a)–(c). In contrast, the $MAPbBr_3$ film prepared using 6 vol% of HBr in the DMF/HBr cosolvent exhibited full coverage and a much smoother surface. However, the $MAPbBr_3$ film surfaces prepared using 8–10 vol% of HBr in the DMF/HBr cosolvent exhibited unwanted cube-shaped crystals on top of the $MAPbBr_3$ films, as shown in Fig. 2(e) and (f). The reason for the formation of these unwanted crystals may be the growth of larger $MAPbBr_3$ crystals at the expense of smaller $MAPbBr_3$ crystals because of their reduced surface energy. In fact, this phenomenon of crystal growth is well-known as Ostwald ripening and can be easily observed in the case of quantum dots.[19,20] In addition, the thickness of the $MAPbBr_3$ film decreased as the concentration of HBr in the DMF/HBr cosolvent increased, as shown in Fig. S2.† As previously mentioned, a greater viscosity yields a thinner $MAPbBr_3$ layer because of the retarded evaporation rate of the solvent; as a result, the crystallization rate will be delayed. As the concentration of HBr in the DMF/HBr cosolvent was increased to 8–10 vol%, unwanted cube-shaped crystals were created; consequently, the overall thickness and roughness increased due to Ostwald ripening. Therefore, the concentration of HBr in the DMF/HBr cosolvent used to spin-coat $MAPbBr_3$ was confirmed to strongly influence the final film morphology and thickness of the $MAPbBr_3$ layers.

To observe other factors that affect the crystallization process, $MAPbBr_3$ films with different annealing times and different spin-speeds used to spin-coat the $MAPbBr_3$ precursor solution using 6 vol% of HBr in the DMF/HBr cosolvent were prepared and their SEM images were compared. The $MAPbBr_3$ films maintained their original morphology, and the Ostwald ripening phenomenon was not observed in the top-view SEM images in Fig. S4 and S5,† despite the annealing time and spin-coating speeds being different. Moreover, the crystal size decreased from 1.5 μm to 500 nm, and the film thickness of an $MAPbBr_3$ single layer with 6 vol% of HBr in the DMF/HBr cosolvent decreased when the spin-coating speed was increased from 1000 rpm to 7000 rpm (Fig. S6†). These results demonstrate that the main factor that influences the morphology of the $MAPbBr_3$ films is the concentration of HBr in the DMF/HBr cosolvent. This simple technique should prove extremely useful as a general method to control the $MAPbBr_3$ crystal size and film thickness with full surface coverage.

3.4 Optical microscopy

Fig. 3(a)–(e) show the EL images of complete PeLED devices with $MAPbBr_3$ films prepared at a constant voltage using different concentrations of HBr in the DMF/HBr cosolvent; a significant correlation between the morphology of the $MAPbBr_3$ films and the EL behavior of complete PeLEDs was observed in the optical microscopy images. The PeLED devices

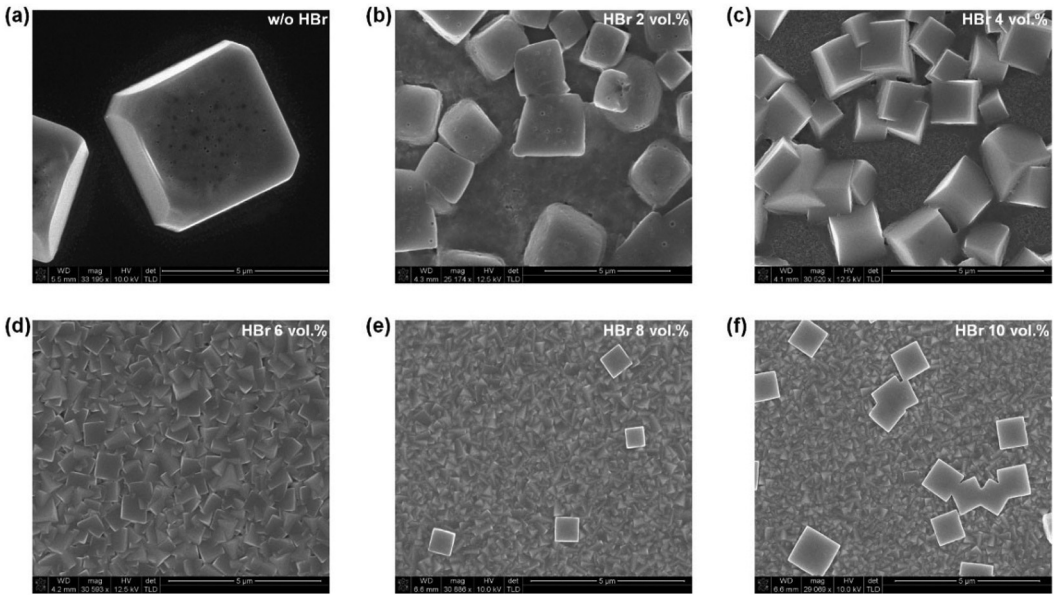

Fig. 2 SEM images of the top surfaces of the $MAPbBr_3$ layers deposited using 0–10 vol% of HBr in the DMF/HBr cosolvent on PEDOT:PSS-coated ITO/glass substrates.

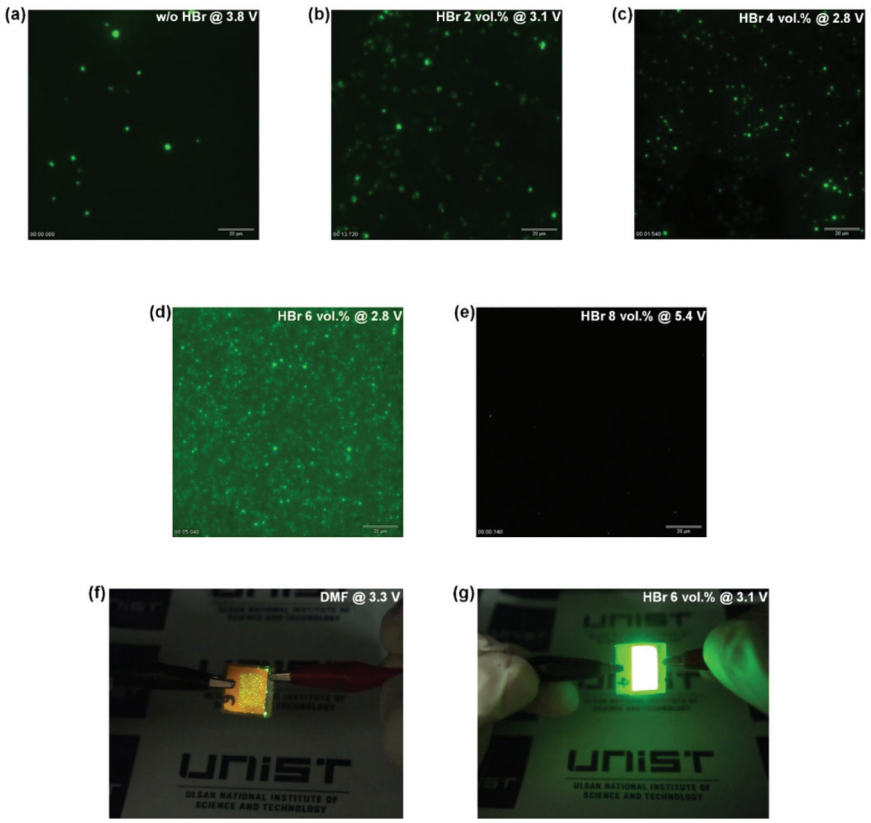

Fig. 3 (a–e) Optical microscopy images of EL from PeLEDs with the $MAPbBr_3$ layers deposited at a constant voltage using different concentrations of HBr in the DMF/HBr cosolvent. (f and g) 1 cm^2-area green EL from $MAPbBr_3$ PeLEDs without and with 6 vol% of HBr in the DMF/HBr cosolvent, respectively.

with an inhomogeneous surface of the $MAPbBr_3$ films with an island-like morphology (0–4 vol% of HBr in the DMF/HBr cosolvent) showed island-like emission (Fig. 3(a)–(c)), whereas the PeLED device with a homogeneous surface of the $MAPbBr_3$ films (6 vol% of HBr in the DMF/HBr cosolvent) showed full coverage of the green emission through the full coverage of the uniform $MAPbBr_3$ film (Fig. 3(d)). However, the PeLED device with $MAPbBr_3$ films deposited using 8 vol% of HBr in the DMF/HBr cosolvent showed minimum island-like light emission even at a higher applied voltage of 5.4 V in Fig. 3(e) because unwanted $MAPbBr_3$ parts were fabricated on top of the thinner $MAPbBr_3$ layer in Fig. S3(e).† Fig. 3(f) and (g) present images of 1 cm^2 emission areas from the $MAPbBr_3$-based PeLED devices without and with using 6 vol% of HBr in the DMF/HBr cosolvent at 3.3 V and 3.1 V biases, respectively; the $MAPbBr_3$-based PeLED prepared using 6 vol% of HBr in the DMF/HBr cosolvent exhibited brighter and more uniform green emission than that without using 6 vol% of HBr in the DMF/HBr cosolvent.

3.5 X-ray diffraction

To confirm the unwanted layer of $MAPbBr_3$ when 8–10 vol% of HBr was used in the DMF/HBr cosolvent, as previously mentioned, the XRD patterns of the resulting films were collected, as shown in Fig. 4(a). The $PbBr_2$ peak and $MAPbBr_3$ peak coexisted in the pattern of the $MAPbBr_3$ film when HBr was not added to the DMF/HBr cosolvent, whereas the intensity of the $PbBr_2$ peak decreased upon the addition of HBr and almost disappeared when the DMF/HBr cosolvent contained 6 vol% of HBr, which is the similar result to previous literature.[18] However, the $PbBr_2$ peak was clearly observed in the pattern of $MAPbBr_3$ films when the DMF/HBr cosolvent contained 8–10 vol% of HBr; these peaks were a consequence of the unwanted $MAPbBr_3$ crystals that resulted from Ostwald ripening during the film growth of the $MAPbBr_3$ layers. The remnant $PbBr_2$ acts as a defect site in perovskite, resulting in an increased rate of non-radiative recombintation and reduced device performance.[21]

3.6 Device performance

The voids and pinholes of the $MAPbBr_3$ film create shunt pathways between the HTL and the ETL, which limits the device performance.[22] As the voltage bias increases, such pinholes would cause dielectric breakdown; thus, the devices with the non-optimized $MAPbBr_3$ layers were observed to easily short-circuit. Fig. S7† shows (a) the current–density *vs.* voltage (*J*–*V*), (b) the luminance *vs.* voltage (*L*–*V*), and (c) the luminous efficiency *vs.* voltage (LE–*V*) characteristics and (d) electro-

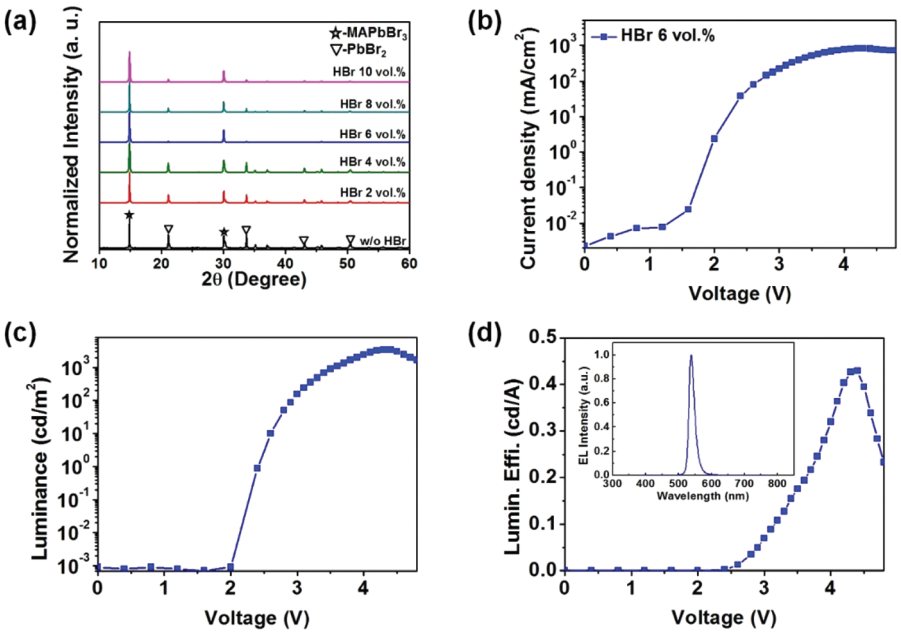

Fig. 4 (a) XRD data of $MAPbBr_3$ films with different volume ratios of HBr in the DMF/HBr cosolvent, where the $MAPbBr_3$ films were deposited onto PEDOT:PSS-coated ITO/glass substrates. Light-emitting characteristics of PeLEDs (ITO/PEDOT:PSS/$MAPbBr_3$ (400 nm)/SPB-02 T(30 nm)/LiF (1 nm)/Ag (80 nm)) with $MAPbBr_3$ prepared using 6 vol% of HBr in the DMF/HBr cosolvent are presented in terms of (b) current density *vs.* the applied voltage (*J*–*V*), (c) luminance *vs.* the applied voltage (*L*–*V*), and (d) luminous efficiency *vs.* the applied voltage (LE–*V*). The inset shows the EL spectrum (530 nm) from the tested PeLEDs.

Table 1 Summary of the device performances of PeLEDs with $MAPbBr_3$ prepared using 6 vol% of HBr in the DMF/HBr cosolvent

Device configuration	L_{max}[cd m^{-2}]@bias	LE_{max}[cd A^{-1}]@bias	PE_{max}[lm W^{-1}]@bias	EQE_{max}[%]@bias
ITO/PEDOT:PSS/$MAPbBr_3$ (HBr 6 vol% in the DMF/HBr cosolvent)/SPB-02 T/LiF/Ag	3490@4.3	0.43@4.3	0.31@4.3	0.10@4.3

luminescence (EL) spectra of PeLEDs with the $MAPbBr_3$ layers deposited using different concentrations of HBr in the DMF/HBr cosolvent. As the concentration of HBr increased up to 6 vol% in the DMF/HBr cosolvent, the current densities were reduced and the luminance values were enhanced due to the formation of uniform and thinner $MAPbBr_3$ films. On the other hand, the current density and the luminance value of the PeLED using 8 vol% of HBr in the DMF/HBr cosolvent dramatically decreased and both 480 nm and 540 nm emission spectra from SPB-02 T and $MAPbBr_3$ were observed due to the creation of unwanted and nonuniform $MAPbBr_3$ layers. The detailed device performances of the PeLEDs are summarized in Table S1.† Next, the PeLEDs with the uniform morphology of $MAPbBr_3$ prepared using 6 vol% of HBr in the DMF/HBr cosolvent were fabricated and measured by changing the spin speed to control the $MAPbBr_3$ films and the thickness of the ETL layer. Fig. 4 shows (b) *J*–*V*, (c) *L*–*V*, and (d) the external quantum efficiency *vs.* voltage (EQE–*V*) characteristics of the optimized $MAPbBr_3$-based PeLED prepared using 6 vol% of HBr in the DMF/HBr cosolvent. The inset image shows the EL spectra of the $MAPbBr_3$ PeLED. The PeLED with the $MAPbBr_3$ deposited using 6 vol% of HBr in the DMF/HBr cosolvent exhibited a maximum luminance of 3490 cd m^{-2} (at 4.3 V) and a luminous efficiency of 0.43 cd A^{-1} (at 4.3 V). The detailed device performance of the optimized $MAPbBr_3$-based PeLED prepared using 6 vol% of HBr in the DMF/HBr cosolvent is summarized in Table 1. It should be noted that the maximum luminance value of our inverted PeLED is the highest value so far presented for inverted structure PeLED devices with $MAPbBr_3$ layers deposited onto PEDOT:PSS coated ITO substrates (Table S2†).

The multilayered structure of polymer LEDs can be challenging to fabricate by a solution process because of the non-orthogonal nature of the solvents used to deposit subsequent layers. In contrast, the multilayered structure of a PeLED with $MAPbBr_3$ and emissive ETL polymers fabricated *via* a solution process can be easily fabricated because the solvents used to deposit the $MAPbBr_3$ (DMF/HBr) and SPB-02 T layers (chlorobenzene) are orthogonal. Such hybrid devices have the advantage of a broad emission, as demonstrated in nanocrystal–polymer hybrid LEDs by changing the thickness of the polymer or the nanocrystal.[23,24] PeLED devices (ITO/PEDOT:

PSS/$MAPbBr_3$ (250–800 nm)/SPB-02 T (55 nm)/LiF/Ag) with different thicknesses of $MAPbBr_3$ were fabricated, as shown in Fig. S7(a).† Two mixed EL emissions from $MAPbBr_3$ and SPB-02 T observed in the PeLEDs with less than 400 nm-thick $MAPbBr_3$ layers. As the thickness of the $MAPbBr_3$ layers was increased in PeLEDs with a fixed thickness of SPB-02 T (55 nm), the EL spectra from SPB-02 T disappeared, and the 540 nm EL spectra for the PeLEDs with a $MAPbBr_3$ thickness between 400 and 800 nm appeared dominant because of the shift of the recombination by charge carriers. Moreover, both 480 nm and 540 nm emission spectra were observed as the thickness of the SPB-02 T layer was increased in the PeLED (ITO/PEDOT:PSS/$MAPbBr_3$ (280 nm)/SPB-02 T (15–55 nm)/LiF/Ag), as shown in Fig. S8(b).† Thus, different colors of the EL emission were realized by controlling the recombination zone, which tuned the thicknesses of the $MAPbBr_3$ and SPB-02 T layers in the organic–inorganic hybrid PeLEDs. Fig. S9† shows the EL spectra of two PeLEDs with different thickness sets of $MAPbBr_3$ and SPB-02 T layers under applied voltages. The clear single mode emission (λ_{max} = 540 nm) with narrow full width half maximum (FWHM) was observed in our optimized PeLED (ITO/PEDOT:PSS/$MAPbBr_3$ (400 nm)/SPB-02 T (30 nm)/LiF/Ag) and it didn't change under applied voltages, which represents that the recombination occurs within the $MAPbBr_3$ layer. Whereas the two mixed emissions of the PeLED (ITO/PEDOT:PSS/$MAPbBr_3$ (280 nm)/SPB-02 T (55 nm)/LiF/Ag) were observed and they changed under applied voltages. The change of the emission under applied voltages indicates that the electron–hole recombination zone in the PeLED (ITO/PEDOT:PSS/green emissive $MAPbBr_3$ (280 nm)/blue emissive SPB-02 T (55 nm)/LiF/Ag) is close to the $MAPbBr_3$/SPB-02 T interface and change spatially with the applied electric field. These results are in agreement with the behavior of emission reported in the literature.[25,26]

It is noted that SPB-02 T is certainly not the best candidate for an ETL because the emission spectrum of SPB-02 T has overlapped with the absorption spectrum of $MAPbBr_3$. To confirm whether the energy transfer between the $MAPbBr_3$ emissive layer and SPB-02 T occurs or not, we used the same thickness condition of Fig. 4(b) (ITO/PEDOT:PSS/$MAPbBr_3$ (400 nm)/SPB-02 T (Merck Co., 30 nm)/LiF/Ag), but replaced the blue-emissive SPB-02 T with green-emissive super yellow (SY, Merck Co., 30 nm) to avoid overlap of the absorption spectrum of $MAPbBr_3$ and the emission spectrum of SY, as shown in Fig. S10.† It is assumed that the electron mobility of SPB-02 T and SY is almost the same because they are fabricated from Merck Co. and have a similar back-bone. The emission spectrum from the PeLED (ITO/PEDOT:PSS/$MAPbBr_3$ (400 nm)/SY (30 nm)/LiF/Ag) is narrow and is the same as that from PeLED (ITO/PEDOT:PSS/$MAPbBr_3$ (400 nm)/SPB-02 T (30 nm)/LiF/Ag)$_3$ in Fig. S10(d),† which represents that the recombination occurs within the $MAPbBr_3$ layer and SPB-02 T acts only as an ETL and does not participate in light emission. Moreover, device performances of two PeLEDs were compared and the luminance and efficiency values of two PeLEDs were almost the same in Fig. S10 and Table S3.† This result clearly supports that a similar device performance is obtained by using polymers with a similar back-bone and electron mobility as an ETL in the PeLEDs of Fig. S10.†

4. Conclusions

In summary, we successfully fabricated highly efficient PeLEDs *via* a uniform and dense $MAPbBr_3$ film with full surface coverage on a PEDOT:PSS-coated ITO/glass substrate by using the optimal concentration of HBr in the DMF/HBr solution. The PeLED with 6 vol% of HBr in the DMF/HBr cosolvent exhibited a maximum luminance of 3490 cd m^{-2} (at 4.3 V) and maximum luminous efficiency levels as high as 0.43 cd A^{-1} (at 4.3 V). The addition of a small amount of HBr to the DMF solvent enables the formation of a dense and uniform $MAPbBr_3$ film with full surface coverage, which facilitates full-coverage EL emission of the fabricated PeLED, resulting in a highly efficient PeLED. By incorporating an electron-transport layer that is itself a luminescent conjugated polymer, uniform green emission from the $MAPbBr_3$/polymer-based PeLED was realized by controlling the recombination region between the $MAPbBr_3$ layer and the luminescent polymer layer by changing the thickness of the SPB-02 T layer used as the ETL. In addition, the EL emission spectra of the $MAPbBr_3$/polymer-based PeLEDs were tuned by controlling the thickness of the perovskite and polymer layers. This approach provides a powerful tool to understand the electroluminescence recombination zone from the emission spectra and a potentially useful approach to apply to broad-band LEDs. Moreover, the prospect of optimizing the processing of perovskite crystallization and the availability of a variety of light-emitting polymers provide a promising future for tailor-made, efficient PeLEDs with desired emission profiles.

Acknowledgements

This study was supported by the Mid-Career Researcher Program (2015R1A2A2A01003263). This work was financially supported by the KIST-UNIST partnership program (1.150091.01/2.150464.01). This work was supported by the Human Resource Training Program for Regional Innovation and Creativity through the Ministry of Education and National Research Foundation of Korea (NRF-2014H1C1A1073051).

Notes and references

1 J. H. Burroughes, D. D. C. Bradley, A. R. Brown, R. N. Marks, K. Mackay, R. H. Friend, P. L. Burns and A. B. Holmes, *Nature*, 1990, **347**, 539.
2 V. L. Colvin, M. C. Schlamp and A. P. Alivisatos, *Nature*, 1994, **370**, 354.
3 Z. K. Tan, R. S. Moghaddam, M. L. Lai, P. Docampo, R. Higler, F. Deschler, M. Price, A. Sadhanala, L. M. Pazos,

D. Credgington, F. Hanusch, T. Bein, H. J. Snaith and R. H. Friend, *Nat. Nanotechnol.*, 2014, **9**, 687.
4 G. Gustafsson, Y. Cao, G. M. Treacy, F. Klavetter, N. Colaneri and A. J. Heeger, *Nature*, 1992, **357**, 477.
5 K. G. Lim, H. B. Kim, J. Jeong, H. Kim, J. Y. Kim and T. W. Lee, *Adv. Mater.*, 2014, **26**, 6461.
6 F. Deschler, M. Price, S. Pathak, L. E. Klintberg, D. D. Jarausch, R. Higler, S. Huttner, T. Leijtens, S. D. Stranks, H. J. Snaith, M. Atature, R. T. Phillips and R. H. Friend, *J. Phys. Chem. Lett.*, 2014, **5**, 1421.
7 A. Kojima, K. Teshima, Y. Shirai and T. Miyasaka, *J. Am. Chem. Soc.*, 2009, **131**, 6050.
8 H. Zhou, Q. Chen, G. Li, S. Luo, T. B. Song, H. S. Duan, Z. Hong, J. You, Y. Liu and Y. Yang, *Science*, 2014, **345**, 542.
9 Y. H. Kim, H. Cho, J. H. Heo, T. S. Kim, N. Myoung, C. L. Lee, S. H. Im and T. W. Lee, *Adv. Mater.*, 2015, **27**, 1248.
10 R. L. Hoye, M. R. Chua, K. P. Musselman, G. Li, M. L. Lai, Z. K. Tan, N. C. Greenham, J. L. MacManus-Driscoll, R. H. Friend and D. Credgington, *Adv. Mater.*, 2015, **27**, 1414.
11 M. Liu, M. B. Johnston and H. J. Snaith, *Nature*, 2013, **501**, 395.
12 J. Burschka, N. Pellet, S. J. Moon, R. Humphry-Baker, P. Gao, M. K. Nazeeruddin and M. Gratzel, *Nature*, 2013, **499**, 316.
13 G. E. Eperon, V. M. Burlakov, P. Docampo, A. Goriely and H. J. Snaith, *Adv. Funct. Mater.*, 2014, **24**, 151.
14 N. K. Kumawat, A. Dey, K. L. Narasimhan and D. Kabra, *ACS Photonics*, 2015, **2**, 349.
15 J. C. Yu, D. B. Kim, G. Baek, B. R. Lee, E. D. Jung, S. Lee, J. H. Chu, K. J. Choi, S. Cho and M. H. Song, *Adv. Mater.*, 2015, **27**, 3492.
16 M. A. M. Sarjidan, H. A. M. Mokhtar and W. H. A. Majid, *J. Lumin.*, 2015, **159**, 134.
17 G. E. Eperon, S. D. Stranks, C. Menelaou, M. B. Johnston, L. M. Herz and H. J. Snaith, *Energy Environ. Sci.*, 2014, **7**, 982.
18 J. H. Heo, D. H. Song and S. H. Im, *Adv. Mater.*, 2014, **26**, 8179.
19 R. D. Vengrenovich, Y. V. Gudyma and S. V. Yarema, *Semiconductors*, 2001, **35**, 1378.
20 W. C. Chan, D. J. Maxwell, X. Gao, R. E. Bailey, M. Han and S. Nie, *Curr. Opin. Biotechnol.*, 2002, **13**, 40.
21 J. H. Heo, H. J. Han, D. Kim, T. K. Ahn and S. H. Im, *Energy Environ. Sci.*, 2015, **8**, 1602.
22 W. Zhang, M. Saliba, D. T. Moore, S. K. Pathak, M. T. Horantner, T. Stergiopoulos, S. D. Stranks, G. E. Eperon, J. A. Alexander-Webber, A. Abate, A. Sadhanala, S. Yao, Y. Chen, R. H. Friend, L. A. Estroff, U. Wiesner and H. J. Snaith, *Nat. Commun.*, 2015, **6**, 6142.
23 S. Coe, W. K. Woo, M. Bawendi and V. Bulovic, *Nature*, 2002, **420**, 800.
24 N. Tessler, V. Medvedev, M. Kazes, S. Kan and U. Banin, *Science*, 2002, **295**, 1506.
25 A. Sadhanala, A. Kumar, S. Pathak, A. Rao, U. Steiner, N. C. Greenham, H. J. Snaith and R. H. Friend, *Adv. Electron. Mater.*, 2015, **1**, 1500008.
26 J. Zaumseil, R. H. Friend and H. Sirringhaus, *Nat. Mater.*, 2006, **5**, 69.